Applied Surface Science 467–468 (2019) 912–925

Contents lists available at ScienceDirect

Applied Surface Science

journal homepage: www.elsevier.com/locate/apsusc

Full Length Article

Influence of silsesquioxane addition on polyurethane-based protective coatings for bronze surfaces

Mohor Mihelčič[a], Miran Gaberšček[a], Gabriella Di Carlo[b], Chiara Giuliani[b], Martina Salzano de Luna[c,d], Marino Lavorgna[c], Angelja K. Surca[a,*]

[a] National Institute of Chemistry, Hajdrihova 19, SI-1000 Ljubljana, Slovenia
[b] Institute for the Study of Nanostructured Materials, National Research Council (ISMN-CNR), Via Salaria km 29,300, 00015 Monterotondo (RM), Italy
[c] Institute for Polymers, Composites and Biomaterials, National Research Council of Italy (IPCB-CNR), P.le E. Fermi 1, 80055 Portici, Italy
[d] Department of Chemical, Materials and Production Engineering, University of Naples Federico II, P.le Tecchio 80, 80125 Naples, Italy

ARTICLE INFO

Keywords:
Bronze
Polyurethane
Protective coating
POSS
Impedance
Infrared spectroscopy

ABSTRACT

Two-component solvent-born polyurethane coatings for the protection of bronze from corrosion were prepared. Trisilanol-heptaisooctyl polyhedral oligomeric silsesquixane (POSS) nanoparticles were exploited to increase the coating protective efficiency. Its improvement was confirmed through a combination of characterisation techniques. In particular, the POSS addition caused an increase of the water contact angle, and an enhancement of the elastic connotation and abrasion resistance of the polyurethane coating. Potentiodynamic polarisation measurements also indicated that the coating containing POSS nanoparticles has an improved protection efficiency. Impedance spectroscopy revealed that the magnitude of low-frequency impedance of polyurethane coatings decreased more for the coating without POSS during exposure in electrolyte for thirty days. *Ex situ* IR reflection-absorption spectroelectrochemistry was exploited to get insight into the degradation of coatings during chronocoulometric charging at anodic potentials. IR reflection-absorption technique was also used to evaluate any possible effect of different stripper solutions on the bronze substrate.

1. Introduction

The development of new protective coatings for bronze surfaces should meet specific demands, some of them being in opposition to each other. The most opposing ones are good protective efficiency and removability, the latter being a criterion of conservation ethics that was a concern of the EU project NANORESTART [1]. From the chemists' perspective, the achievement of both the above-mentioned properties is not a straightforward task. On the one side, a good protection is generally achieved through compact and impermeable coatings that are firmly bonded to the surface of interest. On the other side, excellent adhesion properties prohibit removability aspects [2]. In addition, protective coatings for bronze artworks should be transparent and easy-to-apply. Moreover, outdoor application coatings should be water-insoluble and should withstand changes in temperature, UV radiation and pollutants from atmosphere, including particulate matter.

The tendency of bronze to passivation depends on environmental exposure, type of bronze and its casting quality [3]. The resulting patina may function as a protective layer that also possesses a decorative value [4]. However, in some cases an artificial protection of bronze objects is also desired. Traditionally, the most used commercial products for protection of bronze works include different waxes, such as Soter, acrylic resins, such as Incralac, and their combinations [5]. More recently, other possibilities attracted increased attention of researchers. One of the most often studied anticorrosion solution envisage the use of organic protective films that formed on bronze surfaces during exposure to solutions of benzotriazole and its derivatives [5–8]. Such inhibiting layers are thin, i.e. about some tenths of nm [6]. Alternatively, sol-gel coatings prepared from various organic-inorganic hybrids have also received significant attention [9–13], but they are characterised by a high adhesion to alloy surfaces due to the covalent bonding between silanol and surface hydroxyl groups. Consequently, the promising application of sol-gel coatings is in protection of build materials [14]. Other examples of studied coatings for bronze are based on various polymers, ranging from conductive polymers [5], for which optical transparency is questionable, to fluoropolymers [5], acrylate/methacrylate [15] and polyurethanes [2].

Polyurethanes are characterised by urethane groups (−NH−CO−O−) in their structure, which form in the reaction between polyol resins and polyisocyanates [16,17]. Various polyethers,

* Corresponding author.
E-mail address: angelja.k.surca@ki.si (A.K. Surca).

https://doi.org/10.1016/j.apsusc.2018.10.217
Received 20 April 2018; Received in revised form 9 October 2018; Accepted 26 October 2018
Available online 28 October 2018

polyesters, polyolefins and glycols can represent the polyol precursor, and its characteristics significantly influence the final properties of the obtained polyurethane. The second precursor in the reaction, i.e. one of numerous types of polyisocyanates, is usually quite reactive, and can react with either hydroxyl, amino and carboxylic groups. They are also sensitive to water, the products being amine and carbon dioxide. Advantages of polyurethane coating systems over others are mainly represented by a high mechanical and chemical resistance, excellent lightfastness, weather resistance (especially for aliphatic polyisocyanates) and possibility of curing at room temperature. Such properties, however, do not favour removability. Nonetheless, removability can be achieved either by the use of stripper solvents (possibly with less toxic components compared to dichloromethane) or, modification of the coatings through introduction of polyisocyanates with hydrophilic functionality [2].

Since organic-inorganic sol-gel coatings are characterised by high adhesion, the advantage of their other positive properties can be taken through their incorporation in the polyurethane system. Namely, introduction of organic-inorganic components is an important way to modify mechanical, optical and physical properties of polymer systems [18]. The composite materials can be characterised by strong or weak chemical bonds or even without direct chemical bonding. Strong chemical bonds can be achieved by addition of nanosized polyhedral oligomeric silsesquioxanes (POSS), which by themselves belong to organic-inorganic hybrids [19]. POSS are the smallest silica particles in the nature (< 5 nm) and are characterised by a regular structure [19]. Their formulae can be represented by $(R\text{-}SiO_{1.5})_n$, n = 6, 8, 10, … where R can be different functionality (amino, hydroxyl, alkyl, vinyl, …), which comprises the so-called organic shell of POSS and contributes significantly to characteristic properties of POSS molecules. These organic groups not only determine the properties of POSS, but can also enable bonding of POSS units into the structure of polymers, for example in water-born [20,21] or solvent-born [22–24] systems. Open-cube POSS such as trisilanol-heptaisooctyl-POSS are additional example of molecules that can bind into polyurethane system, as for example into sol-gel matrix [25].

In recent years, various POSS have been largely investigated as potential additives for the improvement of the performances of polymeric matrices [26]. When considering polyurethanes, the enhancement of cohesive forces within the polymer matrix and the presence of a rigid framework closely resembling that of silica can allow the realization of abrasion-resistant coatings with good mechanical properties and high thermal stability [27]. On the other hand, different results have been obtained upon POSS addition depending on a multitude of parameters, such as the mixing procedure [28], the organic groups covalently attached to the silica core [29], and the hydroxyl content and POSS functionality [30]. In this sense, nanoindentation and nanoscratch experiments represent a precise and reliable tool for the evaluation of the surface mechanical properties down to the nanoscale level [31]. As a result, they can be profitably exploited to investigate the effect of POSS addition on the mechanical characteristics of the developed polyurethane coatings.

Insight into the structure of coating and its possible degradation during forced anodic polarisation can be obtained using *ex situ* Near Grazing Incidence Angle (NGIA) infrared reflection-absorption (IR RA) spectroelectrochemical technique. Namely, after chronocoulometric charging of protective coatings at defined potentials, the IR RA spectra are measured giving information on eventual changes in the structure. *Ex situ* IR RA spectra are measured in a NGIA assessment using P polarised light and 80° near grazing angle of incidence. According to the experimental setup, longitudinal optical (LO) modes appeared in IR RA spectra, which are usually shifted to higher wavenumbers with regard to transversal optical (TO) modes that appear in IR absorbance spectra. Interpretation of LO modes is consequently not always straightforward. Such *ex situ* IR RA measurements have already been used in case of coatings prepared on the basis of various sol-gel coatings, also containing POSS [25,32,33]. In these studies, information were obtained on siloxane bond rapture, hydration of coatings and breakage of Si-O-alloy bonds, which bonded sol-gel protective coatings to the substrate alloy. To our knowledge there were no *ex situ* IR RA reports on behaviour of polyurethane coatings.

In the light of the previous considerations, our goal was to produce a polyurethane protective coating for bronze objects that can be removed from surfaces through application of strippers less toxic than conventional ones. IR RA spectroscopy was performed to check if changes of the bronze surfaces occurred during long contact with various stripper solutions. Curing of polyurethane formulations was followed using IR absorbance spectroscopy at room temperature and also at 60 °C. In addition, the influence of trisilanol-heptaisooctyl-POSS additive to the mechanical, surface and electrochemical resistance of coatings was investigated using nanoindentation, contact angles measurements, atomic force microscopy (AFM) and electrochemical tests, such as potentiodynamic polarisation and electrochemical impedance spectroscopy (EIS). *Ex situ* NGIA IR RA spectroelectrochemical measurements were also carried out during forced anodic polarisation to get information on changes in the structure or eventual rupture of bonds.

2. Experimental

2.1. Preparation of materials

Polyurethane solvent-born lacquer U2 was produced from a commercially accessible resin Duroftal VPI 2803/78 BAC (Allnex). In the first step, the resin was dissolved in butyl acetate (20 wt.% of resin in formulation), followed by the addition of trisilanol-heptaisooctyl-POSS (2 wt.%), (purchased from Hybrid plastics) and additives for defoaming and levelling. Tinuvin 1130 and 292 were used as light stabilizers. All components were homogenized using Dispermat®, then a suitable hexamethylene diisocyanate (HDI)-based polyisocyanate (produced by Covestro) was added to start the polymerisation through the reaction between hydroxyl groups of the resin and the isocyanate groups. The molar ratio of resin:isocyanate was 1:1. The formulation was mixed for about 30 min prior to its deposition on bronze disks by using spin-coating (1st step: 5 s, 500 RPM; 2nd step: 60 s, 700 RPM). After deposition, the coatings were thermally treated at 60 °C for 1 h. For comparison, coatings without POSS additive were also prepared, which are referred to as U2-WP.

Commercial Incralac, based on Paraloid B-44 acrylic resin and benzotriazole as corrosion inhibitor, was purchased from Bresciani, Italy (Incralac, Art. 56171). Incralac coatings were produced by diluting 2.4 g of Incralac in 1.6 g toluene. The formulation was poured on the bronze substrate and spread using spin-coating deposition (1st step: 5 s, 500 RPM; 2nd step: 60 s, 1000 RPM).

Bronze rods 85 555 with a diameter of 3 cm were obtained from the foundry Casa Del Bronzo Srl (Brescia, Italy) and cut into disks with thickness of 3 mm. The actual composition of the bronze was determined using inductively coupled plasma optical emission spectrometry (ICP-OES): 4.48 wt.% of Sn, 5.32 wt.% of Zn, 5.24 wt.% of Pb, 0.10 wt.% of Fe, 0.02 wt.% of Ni and the balance being copper. Two different values of surface roughness of the bronze disks were obtained by using two different polishing procedures:

(a) SF-S – flat-lucid surface: First polishing with SiC abrasive paper of P1200 grit, then using two diamond pastes with particle size of 9 and 3 μm.
(b) SF-R – high roughness: Polishing with SiC abrasive paper of P1200 grit.

When not specified, the coatings were deposited on flat-lucid surface (SF1).

Removability of coatings was tested using various solutions. For each experiment, a drop of solution was left for 30 min on the coating

surface and then removed using soft cotton tissue. An aqueous NaOH solution at 0.1 M, a custom-made stripper based on benzyl alcohol, tetraethylene glycol and Triton X100 (stripper I) and commercial Hempel stripper were tested. The components of Hempel stripper that can be recognised from Product Data Sheet are 1,3-dioksolane, dimethoxymethane, isopropanol, oil and methanol. In a typical experiment, properly designed for the laboratory scale, the possible damages that the solutions could make to the bronze surface were investigated by using IR RA spectroscopic technique (see the Instrumental section for details). Namely, an unprotected bronze disk was left for a certain time (1 h, 1 day, 7 days) in solution, then cleaned with acetone or in a flux of dry nitrogen and then the IR RA spectrum was measured in NGIA IR RA specular reflectance accessory (Specac). Water was also checked for its influence on the surface of the bronze.

2.2. Instrumental

IR measurements were made on a Bruker spectrometer IFS 66/S. IR absorbance spectroscopy was used to follow the crosslinking. Specifically, a partially IR transmitting Si wafer was dipped into the corresponding formulation and the so-prepared coating was measured at certain time intervals to follow the crosslinking. Curing at room temperature was followed by measuring IR absorbance spectra after 3 h, 2 days and 3 days. In case of thermal treatment, the coatings were thermally treated at 60 °C for 1 h after deposition, but then left to further curing at room temperature (2, 3 days). An uncoated Si wafer was used as a background. NGIA IR RA specular reflectance accessory (Specac) was applied to detect eventual changes on bronze surfaces after the bronze disks had been soaked in various stripper solutions for certain periods of time (1 h, 1 day, 7 days). The resolution of measurements was 4 cm^{-1}.

Thickness of the coatings was determined using a Taylor Hobson Series II profilometer. The appropriate steps were formed by application of sticky tape on the substrate prior deposition of coatings. After sticky tape removal, the profilometer tip was dragged three times over this step to obtain the average value of thickness.

Theta tensiometer from Biolin Scientific was used for measurements of the static contact angles for water, diiodomethane and formamide at ambient temperature. Microsyringe was used to gently deposit a 4 µL droplet of liquid on the coating. All measurements were repeated at least three times at different positions. The images were captured using a digital video camera and analysed for contact angle measurements using the One Attention software. In addition, free surface energy values were calculated from the average values of the measured static contact angles. They were calculated according to van Oss approach [34] by solving a set of three complete Young equations. Consequently, measurements with three different liquids with known total free surface energy value σ^{tot}, dispersive part σ^{LW}, electron donor component σ^{+} and electron acceptor component σ^{-} were needed.

The coated bronze disks were characterized before and after accelerated corrosion tests. Micro-chemical and morphological characterisations were performed by means of a high brilliance LEO 1530 field emission scanning electron microscope (FE-SEM) apparatus equipped with an energy dispersive X-ray spectrometer (EDS) INCA 450. The analysis by optical microscopy (OM) was carried out by using a Leica MEF4M microscope equipped with a digital camera (Leica DFC 280).

Nanoindentaion and nanoscratch experiments were performed with a NanoTest Platform made by Micro Materials Ltd., equipped with a Berkovich diamond tip with three-side pyramidal geometry. Nanoindentation tests were performed in depth-controlled mode to evaluate the effect of POSS addition on the hardness, H, and elastic modulus, E, of the coatings. In a typical experiment, the applied load was monitored while the diamond tip was driven to indent the surface of the coating for increasing depth values. In order to minimize the viscoelastic effects of the polymer during the unloading stage, the maximum load was kept for 60 s before unloading. In addition, the maximum depth was limited to 200 nm, that is below 10% of the coating thickness in order to avoid substrate interference [35]. For each sample, at least 10 tests were performed to verify reproducibility of the measurements, and the distance between the indentations was set to 50 µm to avoid interaction effects. From the loading-unloading curves, the hardness was evaluated as the indentation maximum load divided by the projected contact area, A, which for a perfectly sharp Berkovich indenter is given by:

$$A = 24.56 h_c^2 \tag{1}$$

where h_c represents the contact depth. The reduced elastic modulus, E_R, of the material was obtained from the unloading curve according to the following relationship:

$$E_R = \frac{\sqrt{\pi}}{2}\frac{S_{max}}{\sqrt{A}} \tag{2}$$

where S_{max} is the slope of the unloading curve at the point of maximum load. Finally, the elastic modulus of the coatings was derived from the reduced elastic modulus by using the following equation:

$$\frac{1}{E_R} = \frac{(1-\nu_S^2)}{E_S} + \frac{(1-\nu_I^2)}{E_I} \tag{3}$$

where E and ν are the elastic modulus and the Poisson's ratio of the material and, the subscripts S and I refer to the tested coating sample and to the indenter, respectively. For calculations, ν_S was taken equal to about 0.5 [36], whereas E_I and ν_I are equal to 1140 GPa and 0.07, respectively [37]. Nanoscratch tests were performed at a fixed velocity of 1 µm s^{-1} with scratch loads progressively increasing up to 50 mN over a scratch length of 2 mm. The measurements were carried out on three different points on each coating and the distance between the consecutive tests was set to 200 µm to avoid interaction effects.

AFM images were recorded over an area of 20 × 20 μm^2 by using a WITec Alpha 300 confocal Raman spectrometer equipped with an AFM microscope. From images, the surface roughness was calculated using the software programme of the instrument according to the following formula:

$$S_q = \sqrt{\frac{1}{MN}\sum_{k=0}^{M-1}\sum_{l=0}^{N-1}[Z(x_k, y_l) - \bar{Z}]^2} \tag{4}$$

Electrochemical polarisation curves were recorded on an Autolab PGSTAT 302 N potentiostat-galvanostat. The protective coating on bronze was positioned as a working electrode with a geometrical area of 1 cm^2 in a flat cell K0235 (Princeton Applied Research). The Pt grid was positioned opposite to the coating and $Ag/AgCl/KCl_{sat}$ reference electrode in the near vicinity of the working electrode. The cell was filled with 0.5 M NaCl electrolyte. The coating was first held at an open circuit potential for 30 min, followed by a linear sweep voltammetry from −1 to 0.5 V with a scan rate of 1 mV s^{-1}. The same flat cell and potentiostat-galvanostat also equipped with Frequency Response Analysis system (FRA) module were used for EIS measurements. Nyquist and Bode plots were determined using frequency range of 10^5 to 10^{-2} Hz and perturbation amplitude of 0.01 V during 30 days of exposure of coatings to 0.5 M NaCl electrolyte.

Ex situ IR RA spectroelectrochemical measurements were made on the above described Autolab PGSTAT 302 N potentiostat-galvanostat and Bruker spectrometer IFS 66/S. The edges and the back of the bronze disk with coating were protected with epoxy shield prepared from Epofix resin and hardener (Struers company). The epoxy protection was left 1 day at room temperature to dry. The coating on bronze was then chronocoulometrically treated at certain potentials (from −0.8 V vs. $Ag/AgCl/KCl_{sat}$) in the electrochemical cell. After each charging the bronze with coating was removed from the cell, washed and transferred to the NGIA IR RA specular reflectance accessory (Specac) in the IR spectrometer. The IR RA spectra were measured

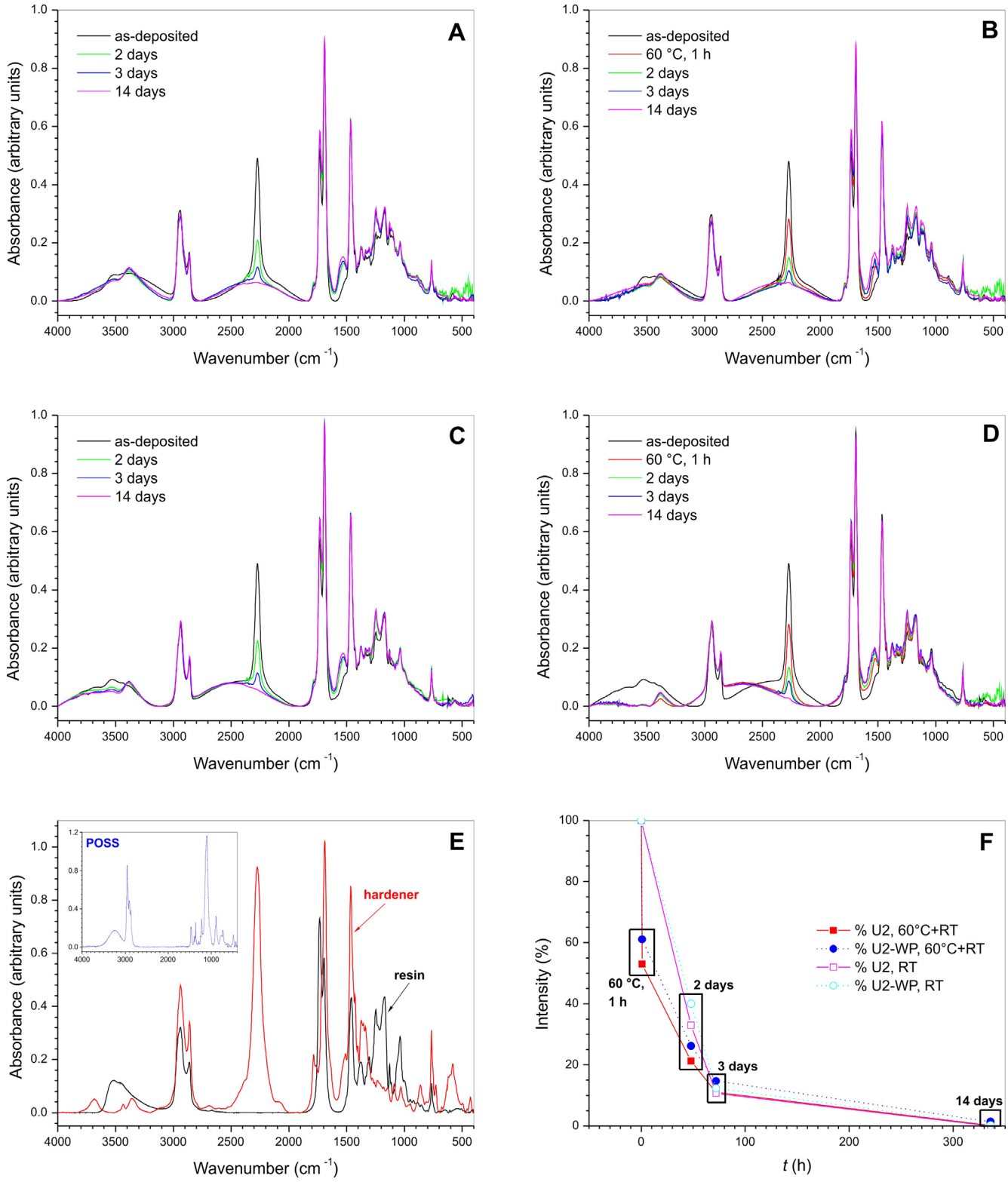

Fig. 1. Absorbance IR spectra of U2 and U2-WP formulations deposited on Si wafer: (A, B) U2 and (C, D) U2-WP; (A, C) curing at room temperature and (B, D) curing at 60 °C for 1 h, followed by measurement after 2, 3 and 14 days at room temperature. (E) IR absorbance spectra of precursor resin and polyisocyanate. Inset: IR absorbance spectrum of trisilanol-heptaisooctyl-POSS. (F) Decrease in intensity of isocyanate mode at 2272 cm^{-1}.

using P polarised radiation and near grazing incidence angle of 80°. The same sample (U2 or U2-WP) was used for measurements at all potentials.

Accelerated corrosion test was carried out by heating at 50 °C the coated bronze disks in a closed glass vessel in the presence of an aqueous 1 M HCl solution. The disks were in contact only with the acid vapour, but not in direct contact with the aqueous solution. The detailed procedure and schematic representation can be found in Ref. [38].

3. Results

3.1. Structure formation

An important question that arises with practical use of polyurethane-based formulations on bronze artworks is how quick the crosslinking occurs. It is desirable that coating forms at room temperature, but thermal treatment at 60 °C is approximation of using a dryer. Consequently, both conditions were tested for U2 and U2-WP formulations using IR absorbance spectroscopy (Fig. 1A–D). The characteristic process of crosslinking consists of the reaction among the hydroxyl groups of the polyurethane resin and polyisocyanate groups of the hardener, their spectra being shown for the sake of comparison in Fig. 1E. This reaction is accompanied by a decrease in the intensity of isocyanate band at 2272 cm^{-1}, the extinction of which indicated the complete consumption of the added polyisocyanate hardener [17]. Fig. 1F indicates the decrease rate of isocyanate vibration mode for different formulations and conditions. The intensity of the isocyanate band recorded immediately after deposition is taken as 100%. The most striking observation is that more than 80% of curing of polyurethane coatings occurred in 2–3 days, no matter if the coatings were first thermally treated at 60 °C (1 h) or simply kept at room temperature. Fig. 1A, B and F showed that a decrease in the intensity of the isocyanate band for about one third occurred for U2 formulation when exposed to 60 °C, but the difference – which is still recognisable after 2 days – levelled off after 3 days at room temperature. No significant differences can be appreciated in the crosslinking behaviour of U2 and U2-WP coatings, the latter being without POSS additive. The concentration of POSS in the U2 coating is low (2 wt.%), therefore its presence in U2 spectra only reflected through low-intensity shoulders of POSS's most notable bands (inset in Fig. 1E). Namely, in the spectra of U2 (Fig. 1A, B) the bands in the ν(C—H) stretching region (2970–2830 cm^{-1}) are shifted to higher wavenumbers, while shoulders could be noted at 1475–1468, 1363, 1227 and 1122–1099 cm^{-1} upon high enlargements of spectra. Accordingly, all the coatings investigated herein were produced by thermal treatment at 60 °C for 1 h and then left at room temperature for one week.

3.2. Morphological and mechanical characterisation of the coatings

The SEM image of U2 coating reveals a fairly homogeneous surface (Fig. 2A). The EDS elemental map reveals a uniform distribution of Si in the polyurethane matrix, thus confirming that POSS nanoparticles did not form detectable aggregates (Fig. 2B). AFM images of U2 and U2-WP were recorded on areas of 20 × 20 μm^2 (Fig. 2C,D). The calculation of surface roughness from AFM images revealed values of 43 and 55 nm for U2 and U2-WP coatings, respectively.

A homogenous dispersion of the nanosized POSS particles and a good interfacial interaction with the polymeric matrix are a prerequisite to ensure an improvement of the mechanical properties of the protective coating. Nanoindentation tests were thus performed to investigate the effect of POSS addition on the mechanical response of the polyurethane-based coatings. Representative load-depth nanoindentation curves are shown in Fig. 3A. The loading-unloading profiles of the U2 and U2-WP coatings share some common characteristics. In particular, the maximum load and the slope of the unloading curve seem not to be affected by the presence of POSS nanoparticles. As a result, the computed values of hardness, which corresponds to the resistance of a material to local surface deformation, and the elastic modulus, which represents the overall stiffness of the polymer network (see equations in the Experimental section) are comparable for the U2 and U2-WP coatings (Fig. 3B).

Actually, the pristine polymeric system, U2-WP coating, already exhibits a high elastic modulus (~6 GPa) and high hardness value (~0.4 GPa). In this case, the POSS addition does not have significant influence on the mechanical properties of the coating, most likely because the rise in cross-linking density due to POSS-polymer matrix reactions is balanced by the increase in the free volume. It is worth noting that this is a non-trivial result, since high performing pristine polyurethane coatings can be also detrimentally affected by POSS addition, which may bring about a decrease in both hardness and elastic modulus [30].

On the other hand, when keeping the applied load constant before unloading, results showed that the penetration of the nanoindenter tip is much more evident in the case of U2-WP coating, suggesting that the deformation mechanism in the two systems is partially different (see Fig. 3A). Nanoindentation tests also allow distinction between recoverable and unrecoverable deformations [39]. In particular, the plasticity index, Ψ, is used to describe the relative plastic/elastic character of a material in the timescale corresponding to the performed nanoindentation measurement, and it is defined as:

$$\Psi = \frac{w_P}{w_P + w_E} \quad (5)$$

where w_P is the area encompassed between the loading and unloading curves and corresponds to the plastic work done during indentation, whereas w_E is the area under the unloading curve and represents the viscoelastic recovery. The analysis of the nanoindentation data reveals that the value of Ψ for the U2 coating is lower than that for U2-WP one (Fig. 3C), indicating that the presence of POSS increases the elastic connotation of the coating, thus eventually improving its ability in spontaneously recovering the deformation.

Additional insight into the mechanical behaviour of the coatings was gained by nanoscratch tests, in which the penetration depth of the indenter tip was monitored for increasing values of applied normal load. A representative output of the measurements is shown in Fig. 4. The analysis of the optical micrographs of the scratch paths highlights that a modest plastic deformation occurs for relatively low loads. On the contrary, at higher loads the formation of pile-up material on either side of the track becomes significant, the effect being much more pronounced in the case of pristine polyurethane coating. This evidence is also confirmed by the profile of the scratch curve, which is clearly more rough for the U2-WP system, indicating that POSS addition improve the abrasion resistance of the polymeric matrix. Further support is also given by the visual identification of the critical load, L_C, that is the load value, at which the primary optically observable fracture phenomenon occurs [40]. Actually, the L_C value for the U2 coating (~11.5 mN) is about 35% higher than that found for the U2-WP one (~8.5 mN), confirming the beneficial effect of POSS particles on the scratch resistance of the developed polyurethane-based systems.

Contact angle measurements were performed to study the water resistance and wettability behaviour of the uncoated bronze surface and of the developed coatings. The static contact angle for water was 104.6° for bronze surface (Table 1), which is close to values that can be found in the literature, for example 105.4° for bronze with Cu(89.0–91.0%), balance Sn [11]. Application of U2 coating on the bronze disk increased the contact angle up to 110.5° (Table 1), further enhancing the hydrophobic connotation of the surface. However, when the coating was prepared without trisilanol-heptaisooctyl-POSS additive (U2-WP coating) the contact angle for water was considerably lower, i.e. 90.3°. Obviously, the high contact angle of U2 coating is a result of the addition of trisilanol-heptaisooctyl-POSS into the polyurethane matrix. The open cage of this kind of POSS nanoparticles, i.e., three available silanol groups, enable the binding into the polyurethane structure via reaction with isocyanate groups of the hardener. This prevents leaching of POSS nanoparticles from the coating matrix. Actually, the pendant POSS groups are distributed throughout the whole matrix of the polyurethane-based U2 coating, also at the surface. The seven corners of each POSS open cage are occupied by isooctyl groups that positively influence the hydrophobicity of the coatings. In fact, it has already been reported that POSS addition influences the hydrophobicity of polymeric coatings, but the extent depends on the functional groups bound to the

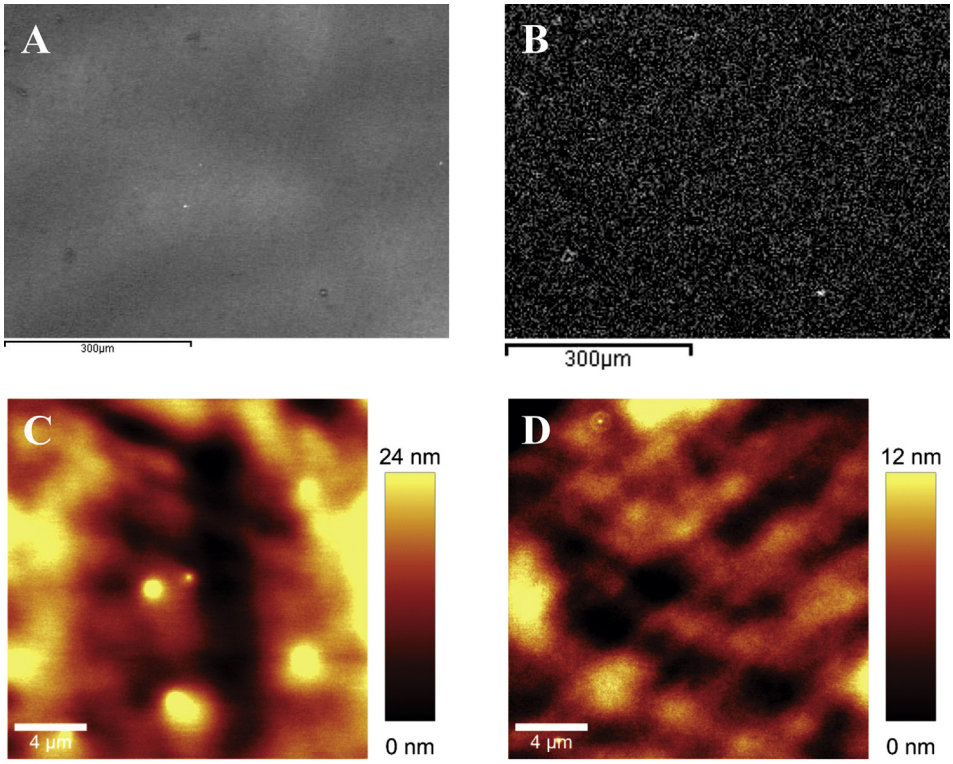

Fig. 2. Surface characterisation of coatings: (A) SEM image of U2 coating, (B) EDS elemental map for Si for U2 coating and AFM images of (C) U2 and (D) U2-WP coatings.

Si—O—Si POSS core [25]. The use of appropriately functionalised POSS cages for the preparation of hydrophobic and even superhydrophobic spectrally selective paints has also been disclosed [41]. The trisilanol-isobutyl-POSS was admixed to increase hydrophobicity, while superhydrophobicity was achieved through addition of aminopropyl-isooctyl-perfluoro-POSS. The variety of possible POSS functionalisations enables the preparation of numerous multifunctional materials and surfaces. Admixture of hydrophobic POSS nanoparticles considerably influences the response of so-prepared materials to wetting. The presence of POSS functionalised with long alkyl chains in the polymeric matrix therefore improves the protection efficiency of such coatings. Similarly, the presence of long alkyl chain of

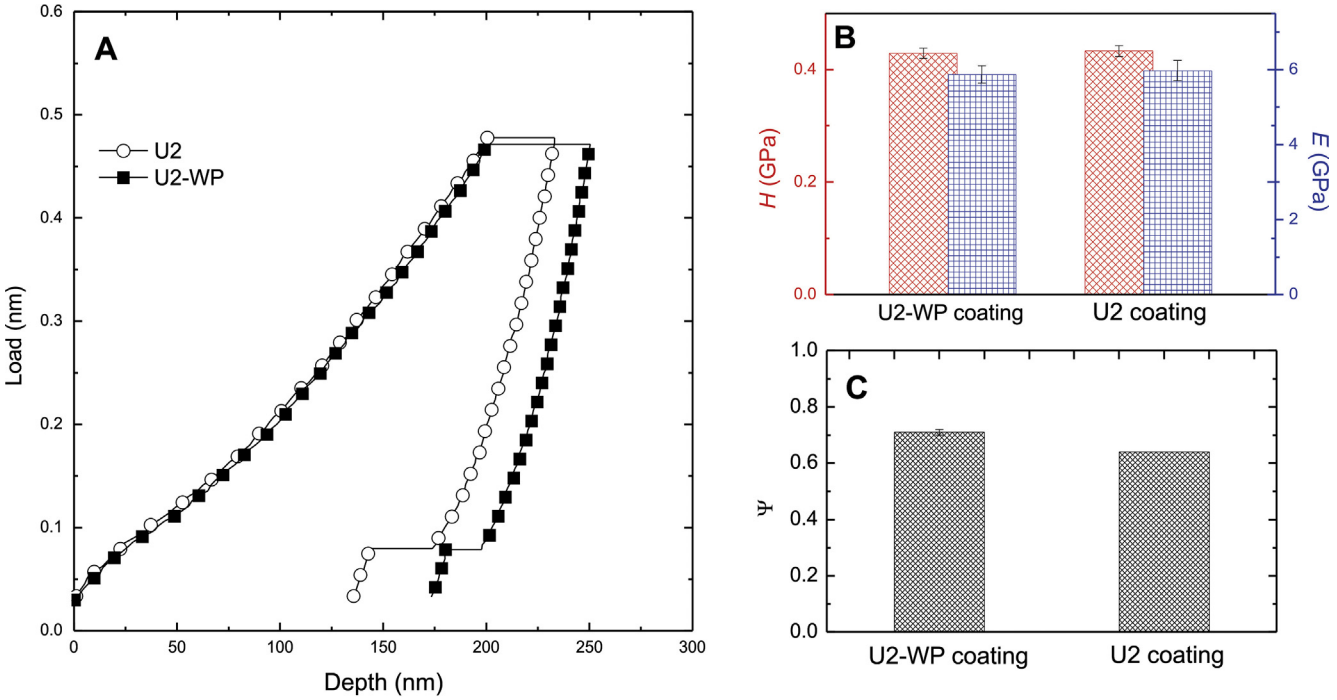

Fig. 3. (A) Representative load-displacement curves, (B) average elastic modulus, hardness and (C) plasticity index obtained through nanoindentation measurements on U2-WP and U2 coatings.

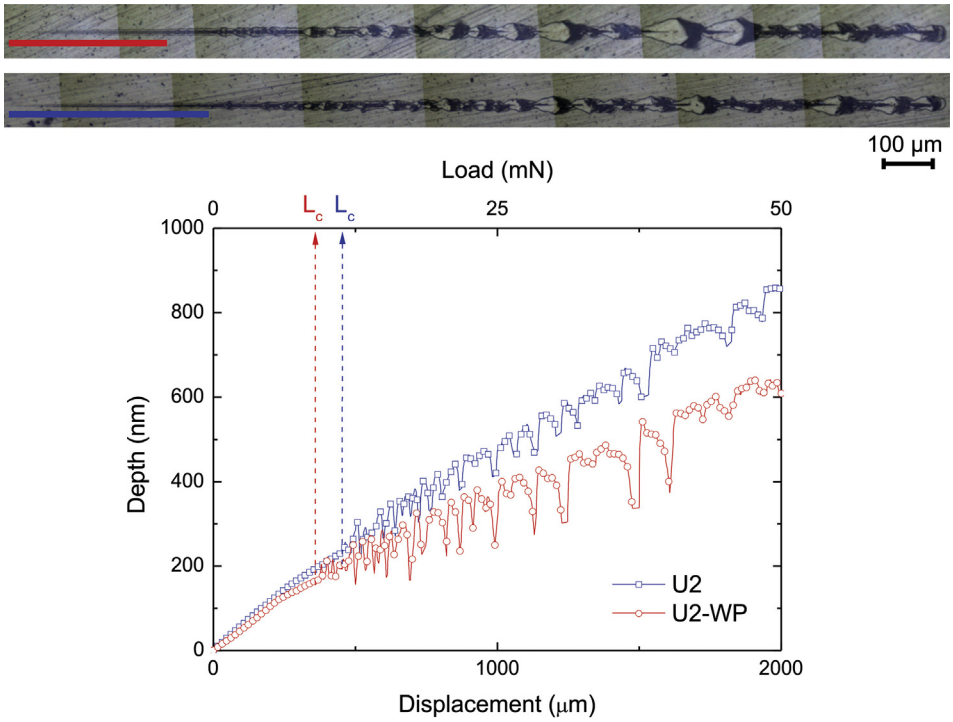

Fig. 4. Representative nanoscratch curves showing the penetration depth of the indenter as a function of displacement (bottom x-axis) and applied load (top x-axis). The corresponding optical micrographs of scratch paths are reported for U2-WP (top image) and U2 (bottom image) coatings.

Table 1
Contact angles for water, formamide and diiodomethane and free surface energy values (in mJ m^{-2}) for bronze, U2 and U2 without POSS additive.

Coating	Θ (°)			τ^+	τ^-	τ^{LW}	τ^{AB}	τ^{tot}
	H_2O	CH_2I_2	$HCONH_2$					
Bronze SF1	104.6	57.9	91.2	1.7	2.7	29.8	4.3	34.1
U2	110.5	59.1	95.4	2.1	1.3	29.1	3.4	32.4
U2 without POSS	90.3	35.7	76.2	1.7	6.3	41.7	6.5	48.2

Θ – contact angle; σ^+ - electron donor component; σ^- - electron acceptor component; d) σ^{LW} – dispersive part; e) σ^{AB} – polar part; f) σ^{tot} – total surface energy value; σ^{tot}, σ^{AB}, σ^{LW}, σ^+, σ^- in mJ m^{-2}.

hexadecyltrimethoxysilane increased the hydrophobicity of cyclotetrasiloxane-based sol-gel coatings [42], or hexamethyldisilozane in alkaline SiO_2 sol increased the contact angle of therefrom prepared coating to a value of ~123° [11].

Consistently with the behaviour of contact angles for water, also the free surface energy values τ^{tot}, calculated on the basis of contact angles for water, diiodomethane and formamide, reflected the presence of POSS additive. Free surface energy value was higher for U2-WP coating (48.2 mJ m^{-2}) than for U2 coating (32.4 mJ m^{-2}), showing that the wettability of the latter coating by water is lower. Actually, any liquid spread spontaneously over the surface of coating when the liquid's surface tension is below the free surface energy of the coating.

3.3. Removability aspects

The use of a protective coating on bronze claims also the possibility of its removal. It was found that both U2 and U2-WP coatings were removable with stripper I and Hempel striper, while 0.1 M NaOH solution was not efficient. The choice of an appropriate stripper solution is important from a toxicological point of view, but should also not affect the surface of the bronze substrate. In a laboratory adapted experiment, the influence of the solutions used for coating removal was checked by soaking the bronze disks in these solutions even for longer periods of time, and then NGIA IR RA spectroscopic measurements were carried out. Results in Fig. 5 reveal that certain bands developed on bronze when exposed to 0.1 M NaOH (Fig. 5A). The bands in these spectra cannot be assigned to $Cu(OH)_2$ [43], although very low-intensity bands at around 3320 and 1062 cm^{-1} may indicate some hydroxylation. Consequently, they were tentatively assigned to stretching ν(CuO−H) and bending Cu−OH vibrations [44]. The presence of Cu_2O oxide LO modes in IR RA spectra has been reported at 640 cm^{-1} [45], 627–619 cm^{-1} [46], 617 cm^{-1} [47] depending on preparation and experimental conditions. Its presence in the spectrum in Fig. 5A can therefore not be excluded (shoulder at 645 cm^{-1}). However, the main bands of the spectrum (1496, 1375, 883 cm^{-1}) can be ascribed to adsorption of carbonate ions from either hydroxide solution or atmosphere. When the bronze disk was soaked in water the characteristic bands of hydroxylation became also visible at 3340 and 1080 cm^{-1}, while the band of Cu_2O started to appear at 621 cm^{-1} (Fig. 5B). The intensities of these bands were, however, significantly lower (different scale) compared to the intensities of the bands obtained by soaking in 0.1 M NaOH solution (Fig. 5A). Consequently, hydroxide solution was considered inappropriate for cleaning.

On the other hand, soaking of bronze disks in the custom-made stripper I (Fig. 5C) and in commercial Hempel stripper (Fig. 5D) did not cause appearance of any bands even after 7 days of soaking. Hence, the utilization of such strippers does not harm the bronze surface during the removal of the solvent-born protective coatings.

Strippers often contain dichloromethane, which was known for its carcinogenic effect and huge hazards in case of ingestion, skin or eye contact. It was long believed that this compound is active in removal of various polymeric coatings. It was shown on the example of polyurethanes that dichloromethane swelled the polyurethane polymer by solvation of carbonyl groups responsible for crosslinking [48]. This produced broadening of Raman carbonyl stretching band, but there is only minimal change in glass transition temperature T_g after drying. However, in series of elimination tests (various combinations of solutions for removal) it was found that addition of weakly acidic phenol to stripper results in significant and irreversible decrease in T_g due to its

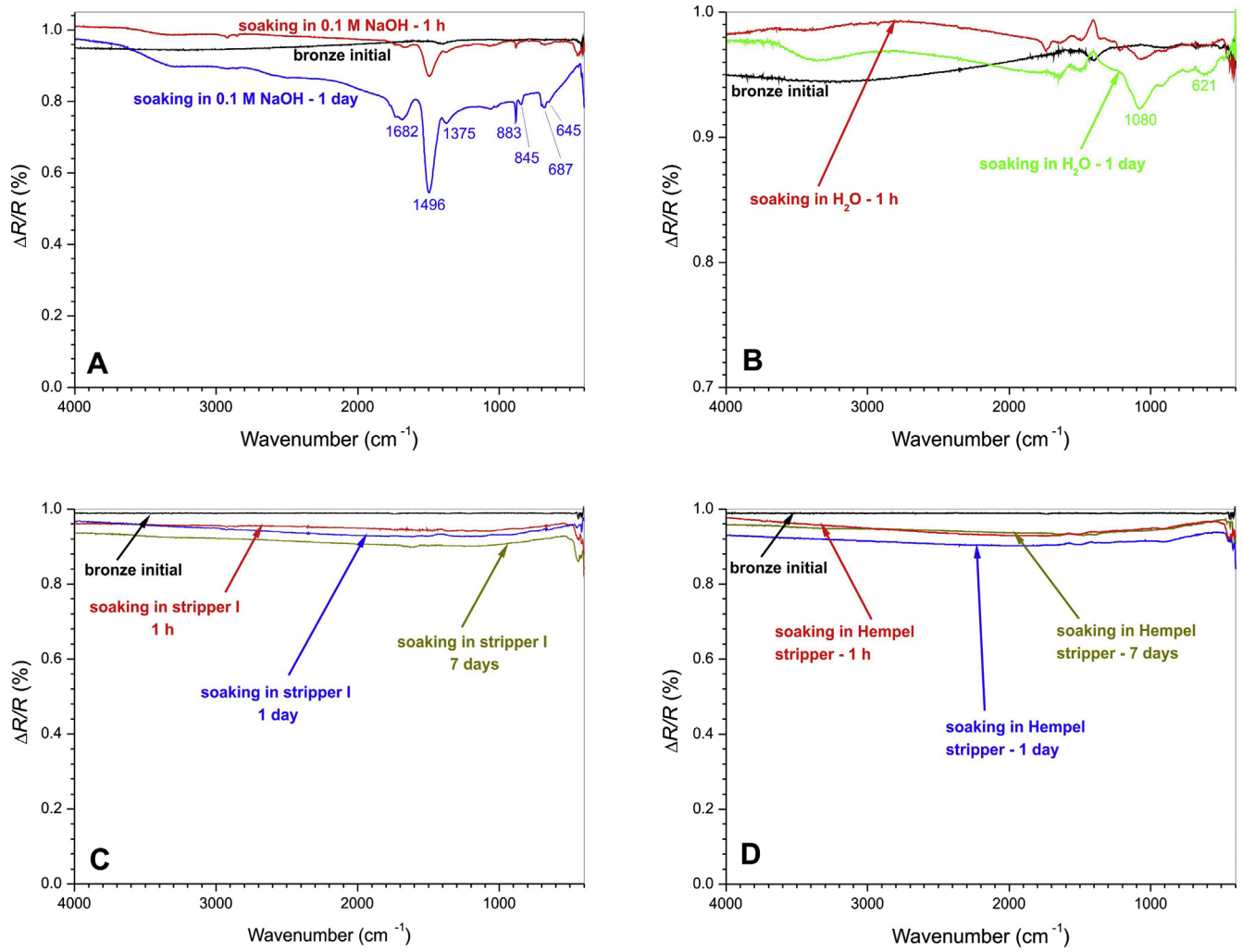

Fig. 5. NGIA IR RA spectra of bronze during 1 h, 1 day and 7 days of soaking in various solutions: (A) 0. 1 M NaOH, (B) H_2O, (C) stripper I and (D) commercial Hempel stripper.

nucleophilic attack on the urethane bonds [48]. Currently, the replacement of such conventional strippers with others on the basis of benzyl alcohol (as stripper I) is already taking place. The main limitation is represented by the time needed for coating removal with benzyl alcohol based strippers, which is usually longer [48]. Such elongation of time is not so questionable for applications on bronze artworks, especially if it is accompanied with the use of compounds that have less health and environmental issues. In our soaking experiments U2 polyurethane coating can be removed using stripper I in 30 min (shorter times were note tested).

3.4. Electrochemical characterisation of coatings

Potentiodynamic polarisation technique is most commonly exploited for the investigation of compact protective coatings for various alloys, but has not been used often in studies of protective coatings for works of art. The reason is the need for highly removable coatings that often cannot bear treatments in aqueous electrolytes (for example, water-soluble coatings used for the in-door protection of bronze). However, when coatings are insoluble in electrolytes, this technique offers quick results, which range coatings relatively with regard to the protective efficiency. Polymeric coatings behave as barriers and their efficiency depend on their thickness. For this reason, for the laboratory experiments the coatings were prepared via spin-coating deposition that enables the preparation of coatings having homogeneous thickness (contrary to the brushing deposition, conventionally adopted in real-life application on works of art). Comparison of potentiodynamic results of U2 and U2-WP with Incralac coatings therefore reveals only direct differences in protection efficiency. This comparison does not comprise other parameters necessary for protection of bronze objects (consistence, application capabilities …). All electrochemical measurements were made in 0.5 M NaCl electrolyte as a simulation of highly corrosive environment.

Potentiodynamic polarisation measurements of U2 and U2-WP coatings showed similar cathodic current density, which decreased for 2–3 orders of magnitude with regard to the uncovered bronze disk (Fig. 6A). The decrease in anodic current density reached even 5–6 orders of magnitude compared to the anodic current density of the bronze itself (Fig. 6A). The protective efficiency of both coatings was good, the protective efficiency of U2 being slightly better compared to U2-WP (i.e. the former showed slightly lower current density). Potentiodynamic technique was additionally used to evaluate the eventual effect of surface roughness on the protection efficiency of coatings. The U2 coating was deposited on bronze substrates with two different roughness values, a rougher SF-R and a smoother SF-S surface. As evident from Fig. 6B, the smoother surface finishing slightly delayed the corrosion processes at the coating|bronze interface. Specifically, a small additional drop in anodic current density was observed. For all other types of measurements SF-S bronze disks were used.

Incralac coatings with thicknesses of 1.1 and 2.2 μm were prepared

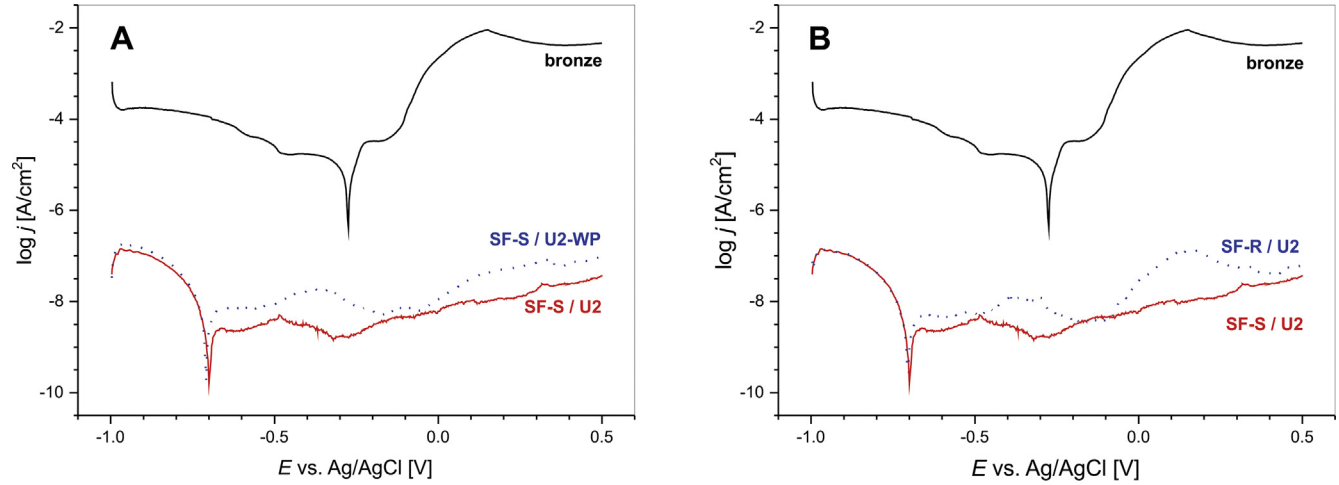

Fig. 6. Potentiodynamic polarisation measurements of: (A) U2 (4 μm) and U2-WP (3.8 μm) coatings deposited on bronze with SF-S grade of roughness and (B) U2 coatings deposited on bronze with two different surface roughness values (SF-S and SF-R).

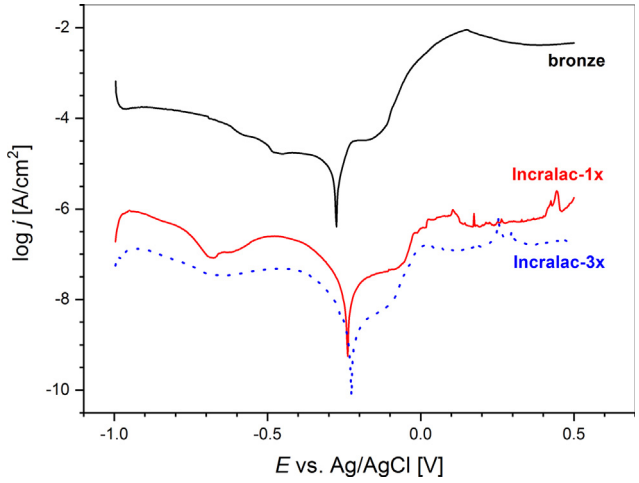

Fig. 7. Potentiodynamic polarisation measurements of Incralac coatings 1× (1.1 μm) and 3× (2.2 μm) spin-coated on bronze with SF-S polishment.

as benchmark products (to be used as reference systems for the evaluation of the protective efficiency of the developed polyurethane-based coatings) and tested with potentiodynamic polarisation technique (Fig. 7). In analogy to U2 and U2-WP coatings, Incralac also behaves as a barrier coating with current densities in the range of 10^{-7} to 10^{-6} A cm^{-2}. The coatings were spin-coated from a 60 wt.% concentrated formulation of Incralac. A concentration of 15 wt.% is usually used by conservators, which during spin-coating deposition leads to thinner coatings, i.e. of about 0.5 μm. Evidently, the potentiodynamic polarisation curves of these coatings usually reveal lower protection efficiency.

The evaluation of corrosion protection of various coatings used in this work was obtained also from EIS measurements (Fig. 8). In the Bode type of representation, the same scale for impedance magnitude (left Y-axis) is used for different coatings and two scales for phase (right Y-axis). In this representation the corrosion protection ability is roughly proportional to the magnitude of impedance at the lowest frequencies. At least two characteristic features emerge rather directly: (i) all coatings (Fig. 8A,B,D) increase the protection ability of pure bronze (Fig. 8C) by several orders of magnitude; (ii) in all coatings the magnitude of EIS spectra generally decreases with immersion time (from 0 h to 30 days), although the values slightly oscillate, especially during the first days. After 30 days the impedance of coated samples drops by about 1 order of magnitude. In pure bronze the impedance slightly increases with time (due to development of surface deposits) but the protection ability becomes even lower after 28 and 30 days.

In order to get a deeper insight into the general differences seen in Fig. 8, we also attempted a more quantitative analysis of selected impedance spectra. For this purpose we selected a representative impedance spectrum for each of the four samples. The corresponding Nyquist plots are shown in Fig. 9. In some cases (see Fig. 9B, blue spectrum), a conventional shape corresponding to three relaxation times for three dynamic processes in surface treated bronzes [49] was observed. However, in most samples pertinent to this study, one impedance arc dominated the impedance response throughout the investigated frequency range (100 kHz–0.01 Hz). In an attempt to make a consistent comparison between the four samples, we first needed to identify the physical background of the different observed processes. Specifically, we noticed that the typical capacitances associated with the predominating arc in U2, U2-WP, as well as in the Incralac (Fig. 8D) samples were of the order of 10^{-8}F per 1 cm^2 of electrode surface area (this value was roughly evaluated from the values of corresponding CPE elements used in the fits). By contrast, the typical capacitance for the arc observed in pure bronze was on the order of 10^{-5} F cm^{-2}, which is most likely associated with the double layer capacitance. Values of capacitances of the order of 10^{-8} to 10^{-9} F cm^{-2}, however, are typically observed in surface coatings of thicknesses in the micrometer range [50]. This can be verified by a simple calculation, in which the film capacitance, C, is approximated by the Eq. (6) for a parallel plate capacitor:

$$C = \varepsilon\varepsilon_0 \frac{A}{L} \tag{6}$$

where ε is the average dielectric constant of the film, ε_0 is the permittivity of vacuum ($8.85 \cdot 10^{-12}$ A s V^{-1} m^{-1}), A is the electrode surface area and L is the average coating thickness. Indeed, taking an arbitrary dielectric constant of 10, a coating thickness of 10^{-6} m and a surface area of 10^{-4} m, one gets for the capacity a value of $8.85 \cdot 10^{-9}$ F, i.e. in the range mentioned above.

In the present case, the only unknown parameter in Eq. (6) is the value of the coating dielectric constant. Thus, by inserting the measured arc capacitances and the coating geometrical data into Eq. (6), we get the following average dielectric constants for the coatings U2, U2-WP and Incralac: 22.6, 32.9 and 53.3, respectively. These relatively high values reflect a relative high water (i.e. aqueous based solution) content due to gradual soaking during exposure [15] and/or inherently high dielectric constant of the main coating components. If the former effect prevails, one can roughly conclude, that the least water has penetrated into U2, followed by U2-WP and thin Incralac coating. Such statement

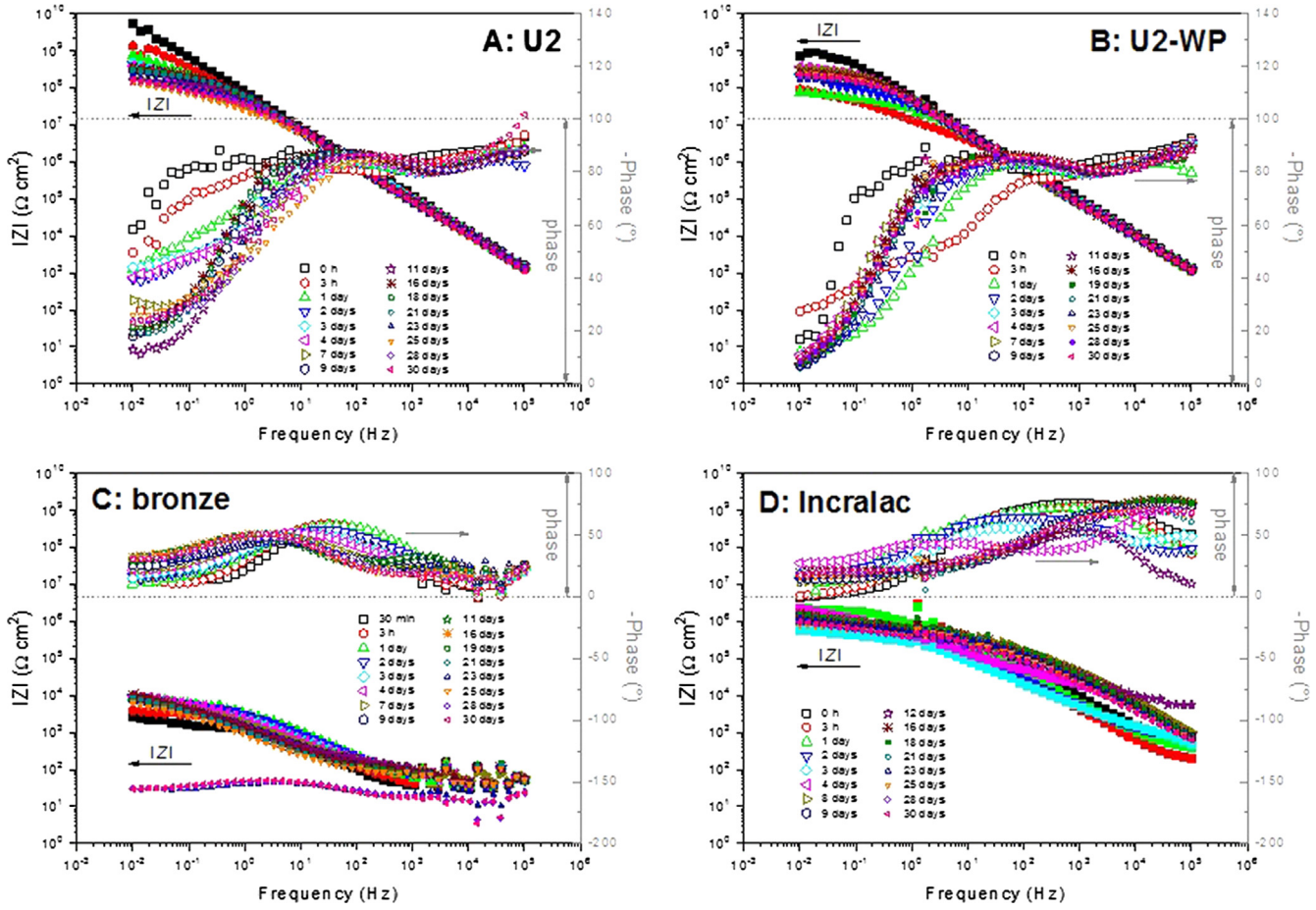

Fig. 8. Bode plots of various protective coatings and bronze: (A) U2 (4 μm), (B) U2-WP (3.8 μm), (C) bronze and (D) Incralac coating (1.9 μm). Left and right Y axes show the magnitude of impedance and phase angle, respectively.

agrees with the easiest removability of Incralac among all three coatings. Moreover, it confirms the initially mentioned compromise that has to be achieved between the protective efficiency and removability.

Additional information that can be extracted from single-arc analysis of these three coatings is the average coating resistivity (ρ [Ω m]). Following the same assumptions as in derivation of Eq. (6), one gets the following formula for thin film resistivity:

$$\rho = R\frac{A}{L} \tag{7}$$

where R is the measured resistance due to impedance arc, and A and L have the same meaning as before. Using Eq. (7) one gets the following values of ρ for U2, U2-WP and Incralac: 2.95×10^{10} Ω m, 5.42×10^{9} Ω m and 4.21×10^{9} Ω m, respectively. In other words, the average coating resistivity of U2 is about six times greater than that of U2-WP

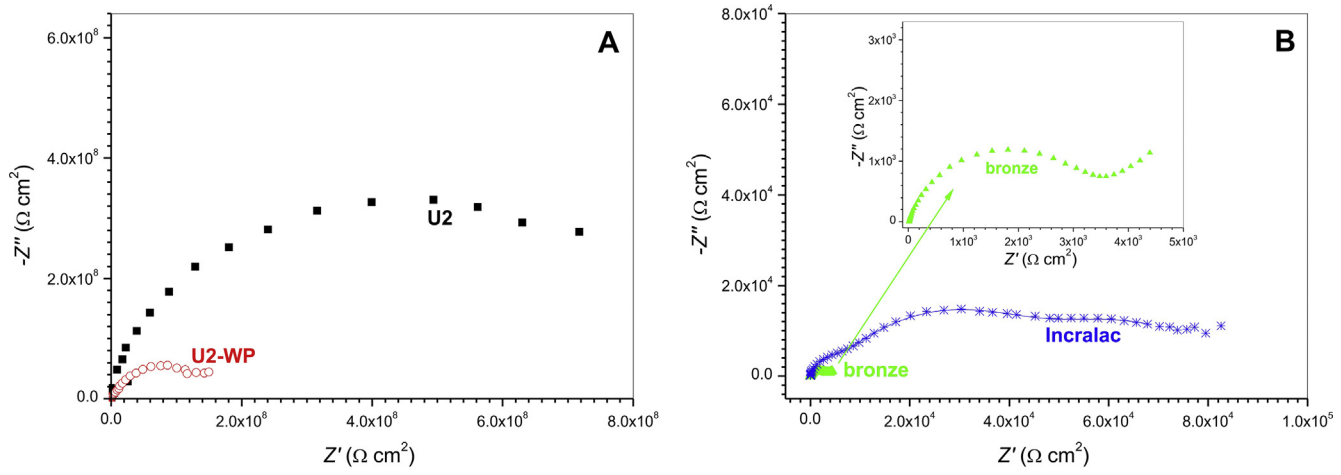

Fig. 9. Typical Nyquist plots of various protective coatings and of pure bronze: (A) U2 and U2-WP, (B) Incralac coating and pure bronze. Inset in panel B shows enlarged Nyquist plot of bronze. The solid line running through measured points of Incralac sample represent a fit using an equivalent circuit proposed by Muresan et al. [49] consisting of three hierarchically positioned R-CPE pairs. The other three spectra were roughly evaluated using a single R-CPE element (see the main text for more details and comments).

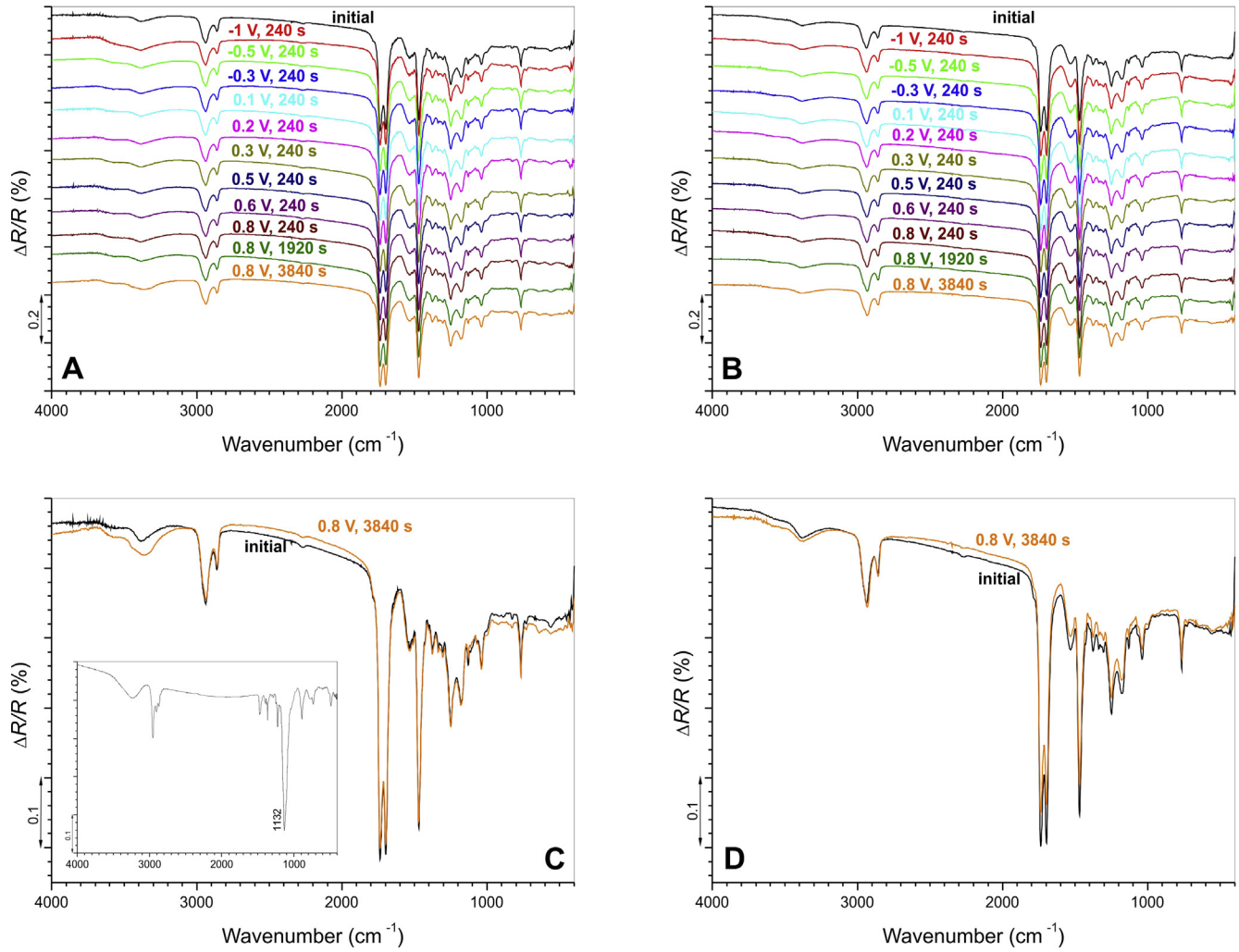

Fig. 10. *Ex situ* IR RA spectroelectrochemical measurements of coatings: (A, C) U2 and (B, D) U2-WP. (A, B) represent whole set of spectra measurements and (C, D) initial spectrum together with the spectrum recorded at the highest potential of 0.8 V vs. Ag/AgCl/KCl_{sat} (scaled-up to ν(C—H) region).

and seven times greater than in Incralac. These values may be used as a rough estimation of protection ability of the coatings if comparable geometry is assumed (i.e. similar electrode surface area and thickness). At least partly, this ability could be connected to the aforementioned value of the average dielectric constant that reflects the ability to prevent excessive water uptake.

3.5. *Ex situ IR RA spectroelectrochemical characterisation*

To support the findings of electrochemical measurements, *ex situ* IR RA spectroelectrochemical measurements were taken during chronocoulometric charging of coatings towards more and more anodic potentials (Fig. 10). Such measurements enable the identification of the bonds that are the most prone to rapture and consequently to lower protection effectivity of the coatings. The measured spectra for either U2 or U2-WP coatings (Fig. 10A, B) do not show obvious changes during electrochemical treatment. Consequently, the initial and the most polarised spectra are compared in Fig. 10C, D and the spectra were scaled-up according to stretching ν(C—H) modes.

Comparison of initial U2 and U2-WP spectra (Fig. 10C, D) does not reveal any major difference. The content of trisilanol-heptaisooctyl-POSS in formulations was small and contributes only in the appearance of a shoulder band at approximately 1110 cm^{-1} in the initial spectrum of U2. The origin of this shoulder is the most intense siloxane band at 1135 cm^{-1} in the IR RA spectrum of trisilanol-heptaisooctyl-POSS (inset in Fig. 10C).

The subsequent comparison of the *ex situ* IR RA spectra of U2 and U2-WP obtained initially and after polarisation to 0.8 V vs. Ag/AgCl/KCl_{sat} (Fig. 10C, D) showed that the change in intensity of broad OH band between 3600 and 3000 cm^{-1} can be ascribed to hydration of the coating. That hydration of coatings occurred has already been found with EIS measurements (Figs. 8 and 9). Moreover, the comparison of *ex situ* IR RA spectra reveals a decrease of about 3% in intensity of U2 coating's bands in the spectral region 2000–1000 cm^{-1} due to slow dissolution of the coating. Such decrease in intensity of bands is considerably larger, i.e. up to 10%, for U2-WP coatings (Fig. 10D). This result undoubtedly reflected that the U2-WP coating possesses a lower protective efficiency, which is a consequence of the absence of trisilanol-heptaisooctyl-POSS in the structure. In the literature, we could not found any *ex situ* IR RA measurements of polyurethane coatings; consequently the comparison was not possible. *Ex situ* IR RA spectroelectrochemical measurements can be predominantly found for various sol-gel protective layers, among them some containing different POSS compounds [25,32,33]. For these sol-gel coatings it was confirmed that POSS positively influences their protective efficiency.

3.6. *Accelerated corrosion tests*

To assess the protective efficiency of the coatings, potentiodynamic polarisation and EIS measurements were carried out using a 0.5 M NaCl

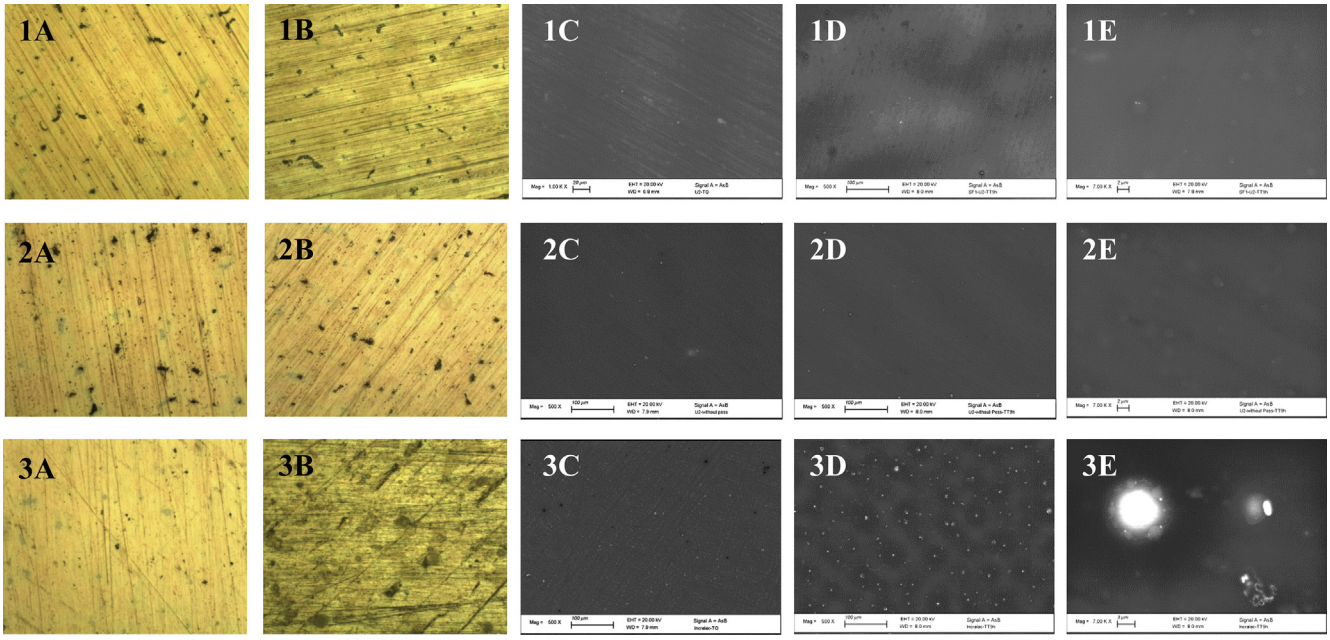

Fig. 11. Accelerated corrosion test: (A, B) optical micrographs and (C–E) FE-SEM images of the bronze disks coated with U2 coating (3.1 μm) (1), U2-WP coating (3.5 μm) (2) and commercial Incralac (1.9 μm) (3). The coatings were characterized before (A, C) and after (B, D, E) corrosion treatment with acid vapour for 9 h.

solution as electrolyte. Moreover, tailored accelerated corrosion test has been developed. This test was originally developed for water-soluble protective coatings and nano-structured diamond-like carbon (DLC) coatings, which are also very interesting from the conservation point of view [38]. The accelerated corrosion test consists of mild heating (50 °C) of the coated bronze substrates in the presence of HCl water vapours. These tests provide information about the aging in conditions that simulate in an accelerated way the exposure of the coated bronze substrates to the direct contact with water (rain) and to some aggressive species present in the atmosphere. Sodium chloride and hydrochloric acid were selected as model aggressive agents because they contain chloride species that promote corrosion processes in copper based alloys [51–56]. In particular, chloride ions with moisture and oxygen are responsible for the well-known “bronze disease”, the cyclic copper corrosion process that can irreversibly compromise the conservation status of copper-based alloys [54]. The experiments were designed in the way that the coatings were characterized before and after the exposure to acid vapour at 50 °C by optical and FE-SEM microscopy to evaluate the protective properties. The micrographs of U2, U2-WP and commercial Incralac coatings are reported in Fig. 11.

Accelerated corrosion test showed that the U2 coating after the corrosion test for 9 h was still stable, transparent and there was no evidence of the formation of corrosion products (Figs. 11, 1B, D, E). The optical micrographs in Fig. 11, 1A, B confirmed that the coating remained unchanged after the corrosion treatment in acid vapour, thus demonstrating the efficiency of the coating in the inhibition of corrosion processes. The findings for U2-WP coating, i.e. polyurethane-based coating without POSS, were quite similar (Fig. 11, 2A–E). In the case of bronze disk coated with commercial Incralac, the accelerated corrosion treatment led to the loss of the coating transparency and to the modification of the alloy substrate appearance (Figs. 11, 3A, B). FE-SEM images after the corrosion treatment clearly showed the absence of damages in the U2 and U2-WP coatings (Figs. 11, 1D, E and 2D, E), whereas defects and corrosion products containing chloride were detected in the Incralac coating (Figs. 11, 3D, E). These findings confirm the results of electrochemical impedance spectroscopy, and the opposing relation between protective efficiency and removability.

4. Discussion

A combination of spectroscopic, electrochemical, nanoindentation and microscopic techniques were exploited to investigate the potential use of solvent-born polyurethane coatings for protection of bronze surfaces. All the adopted characterisation techniques confirmed that the protection effectivity opposes to the removability criterion. Since polyurethanes are known for their high mechanical, chemical and weather resistance, their firm structure can be influenced by the addition of hydrophilic polyisocianates. Consequently, coatings can be removed using organic stripers. An experiment was designed for laboratory scale studies to test whether various stripper solutions affect the surface of bronze. In particular, bronze disks were soaked in different stripper solutions (up to 7 days), and then NGIA IR RA spectroscopy was used for the analysis of the surface. None of the bands evolved when organic strippers were applied (Fig. 5). An important drawback of polyurethane coatings for protection of bronze objects is the long curing time (some days to 1 week) at room temperature (Fig. 1).

Organic-inorganic nanoparticles, i.e. trisilanol-heptaisooctyl-POSS, were included in polyurethane U2 coatings. EDS showed that the nanoparticles distribute homogeneously in the U2 coating (Fig. 2B). The load-depth nanoindentation curves revealed that hardness and elastic modulus were not affected by addition of trisilanol-heptaisooctyl-POSS (Fig. 3A, B). On the other hand, the plasticity index, showing the ability of material to spontaneous recovering after deformation, was higher for U2 coating than for U2-WP coating without nanoparticles (Fig. 3C). Moreover, abrasion resistance and water contact angle improved by trisilanol-heptaisooctyl-POSS addition (Fig. 4, Table 1).

The electrochemical characterisation, i.e. potentiodynamic curves (Fig. 6) and EIS spectroscopy (Figs. 8 and 9), revealed only slightly lower protection efficiency of U2-WP coatings with regard to U2 coatings. The protective efficiency of Incralac coatings was somewhat lower (Figs. 7–9), the consequence of which is its better removability. All coatings were produced using spin-coating deposition to realize coatings with uniform thickness for reliable electrochemical characterisation. Consistent results about protective efficiency were obtained also with accelerated corrosion test (Fig. 11). All these results refer to barrier properties of coatings and do not comprehend other well-known advantages of Incralac that have led to its widespread application.

Coupling of electrochemical treatment with spectroscopic characterisation can enable insight into the evolution-degradation of structure of polyurethane coatings with treatment at increasing anodic potential (Fig. 10). These *ex situ* NGIA IR RA measurements showed the hydration of both coatings, but the decrease in intensity of bands was larger for U2-WP coating. This indicated its inferior behaviour compared to U2 coating.

The studies have already been directed toward more applicative direction, including the optimisation of components and consistency of formulations to enable deposition by brushing. In future, other bronze substrates with different chemical composition will be tested, also with much higher surface roughness and patina to better approach real conditions of many artworks.

5. Conclusions

Protective U2 coatings for bronze surfaces were produced as two-component solvent-based formulations based on polyurethane resin. For laboratory scale investigations, the formulations were deposited on bronze disks using spin-coating technique. Removability of coatings was achieved through the use of hydrophilic polyisocyanate hardener.

The aim of this work was also to study the influence of trisilanol-heptaisooctyl-POSS addition to formulations with respect to mechanical properties and protective efficiency. The increased protective efficiency of POSS-enriched coatings (U2 vs. U2-WP coatings) was confirmed by contact angle measurements, potentiodynamic polarisation, impedance spectroscopy and *ex situ* IR RA spectroelectrochemistry. SEM analysis showed that U2 coating is highly homogeneous and the EDS analysis revealed that Si (originating from POSS) is uniformly distributed into the polymer matrix. Increased hydrophobicity of U2 coatings with respect to U2-WP coatings was indicated by contact angles of 110.5° and 90.3°, respectively.

Nanoindentation measurements revealed that the pristine polyurethane U2-WP coating already possesses high elastic modulus and hardness, which are not noticeably affected by POSS addition. On the other hand, the U2 coating exhibits a lower plasticity index, suggesting that the presence of the POSS improves the ability of the coating in spontaneously recovering the deformation. Nanoscratch tests highlighted that U2 coating is characterized by higher critical load (L_c) and less rough scratch profile than the U2-WP coating, indicating that the addition of POSS improves the abrasion resistance of the developed U2 coating.

Impedance spectroscopy indicated that the protective ability of polyurethane-based coatings with POSS at low polarisations was slightly higher than that of coating without POSS. Comparison of polyurethane coatings with Incralac benchmark showed that the average dielectric constant of Incralac was higher, i.e. 53.3, versus 32.9 and 22.6 for polyurethane coatings without and with POSS. Higher value reflects the larger water uptake. These measurements refer strictly to protective effectivity of coatings as determined by electrochemical techniques. Other properties of Incralac (consistency etc.) that contributed to its widespread use do not reflect through electrochemical experiments. Accelerated corrosion test also confirmed the electrochemical findings.

Ex situ IR RA measurements showed that during polarisation at high anodic potentials larger decrease in intensity of bands in the spectral range 2000–1000 cm^{-1} was noted for U2-WP than U2 coatings. This confirms the positive influence of POSS addition on protective efficiency. IR RA technique also showed that the surface of bronze after soaking in sodium hydroxide solution or water changes, while remained unchanged after application of a custom-made stripper based on benzyl alcohol.

Acknowledgements

This study has received funding from the European Union's Horizon 2020 research and innovation programme under grant agreement No. 646063 (NANORESTART, NANOmaterials for the RESToration of works of ART). Allnex company is acknowledged for providing us their resin products. Department of Analytical Chemistry, National Institute of Chemistry, is acknowledged for elemental analysis of bulk bronze substrate. The authors also thank Mr. Mario De Angioletti for the technical support during nanoindentation analyses. Dr. Cristina Riccucci and Dr. Marianna Pascucci are kindly acknowledged for the SEM and optical analysis.

Appendix A. Supplementary material

Supplementary data to this article can be found online at https://doi.org/10.1016/j.apsusc.2018.10.217.

References

[1] NANOmaterials for the REStoration of works of ART (NANORESTART), EU Project, Grant Agreement No. 646063 (2015–2018).
[2] T.J. Shedlosky, A. Huovinen, D. Webster, G. Bierwagen, Development and evaluation of removable protective coatings on bronze, Proc. Met. 2004, National Museum of Australia Canberra ACT, Canberra, 2004, pp. 400–413.
[3] L.B. Brostoff, Coating Strategies for the Protection of Outdoor Bronze Art and Ornamentation, Ph.D Thesis University of Amsterdam, 2003.
[4] R. Walker, Corrosion and preservation of bronze artifacts, J. Chem. Educ. 57 (1980) 277–280, https://doi.org/10.1021/ed057p277.
[5] G. Bierwagen, T.J. Shedlosky, K. Stanek, Developing and testing a new generation of protective coatings for outdoor bronze sculpture, Prog. Org. Coatings 48 (2003) 289–296, https://doi.org/10.1016/j.porgcoat.2003.07.004.
[6] G. Brunoro, A. Frignani, A. Colledan, C. Chiavari, Organic films for protection of copper and bronze against acid rain corrosion, Corros. Sci. 45 (2003) 2219–2231, https://doi.org/10.1016/S0010-938X(03)00065-9.
[7] K. Rahmouni, H. Takenouti, N. Hajjaji, A. Srhiri, L. Robbiola, Protection of ancient and historic bronzes by triazole derivatives, Electrochim. Acta 54 (2009) 5206–5215, https://doi.org/10.1016/j.electacta.2009.02.027.
[8] T. Kosec, A. Legat, I. Milošev, The comparison of organic protective layers on bronze and copper, Prog. Org. Coatings 69 (2010) 199–206, https://doi.org/10.1016/j.porgcoat.2010.04.010.
[9] E. Bescher, J.D. Mackenzie, Sol-gel coatings for the protection of brass and bronze, J. Sol-Gel Sci. Technol. 26 (2003) 1223–1226, https://doi.org/10.1023/A:1020724605851.
[10] C. Chiavari, A. Balbo, E. Bernardi, C. Martini, F. Zanotto, I. Vassura, M.C. Bignozzi, C. Monticelli, Organosilane coatings applied on bronze: influence of UV radiation and thermal cycles on the protectiveness, Prog. Org. Coatings 82 (2015) 91–100, https://doi.org/10.1016/j.porgcoat.2015.01.017.
[11] E. Kiele, J. Senvaitiene, A. Griguceviciene, R. Ramanauskas, R. Raudonis, A. Kareiva, Application of sol-gel method for the conservation of copper alloys, Microchem. J. 124 (2016) 623–628, https://doi.org/10.1016/j.microc.2015.10.003.
[12] F. Zucchi, Sol-gel coatings for the preservation of metallic heritage artefacts, in: A. Dillmann, P. Watkinson, D. Angelini, E. Adriaens (Eds.), Corrosion and Conservation of Cultural Heritage Metallic Artefacts, Woodhead Publishing Limited, Oxford, 2013, pp. 540–551, , https://doi.org/10.1533/9781782421573.5.540.
[13] G. Masi, A. Balbo, J. Esvan, C. Monticelli, J. Avila, L. Robbiola, E. Bernardi, M.C. Bignozzi, M.C. Asensio, C. Martini, C. Chiavari, X-ray photoelectron spectroscopy as a tool to investigate silane-based coatings for the protection of outdoor bronze: the role of alloying elements, Appl. Surf. Sci. 433 (2018) 468–479, https://doi.org/10.1016/j.apsusc.2017.10.089.
[14] A. Mauko Pranjić, J. Ranogajec, L. Škrlep, A. Sever Škapin, S. Vučetić, K. Malovrh Rebec, J. Turk, Life cycle assessment of novel consolidants and a photocatalytic suspension for the conservation of the immovable cultural heritage, J. Clean. Prod. 181 (2018) 293–308, https://doi.org/10.1016/j.jclepro.2018.01.087.
[15] N.A. Swartz, T.L. Clare, Understanding the differences in film formation mechanisms of two comparable solvent based and water-borne coatings on bronze substrates by electrochemical impedance spectroscopy, Electrochim. Acta 62 (2012) 199–206, https://doi.org/10.1016/j.electacta.2011.12.015.
[16] A. Reghunadhan, S. Thomas, Polyurethanes: structure, properties, synthesis, characterization, and applications, in: S. Thomas, J. Datta, J.T. Haponiuk, A. Reghunadhan (Eds.), Polyurethane Polymers: Blends and Interpenetrating Polymer Networks, Elsevier Inc., 2017, pp. 1–16, , https://doi.org/10.1016/B978-0-12-804039-3.00001-4.
[17] M. Špirkova, J. Pavličević, A. Strachota, R. Poreba, O. Bera, L. Kapralkova, J. Baldrian, M. Šlouf, N. Lazić, J. Budinski-Simendić, Novel polycarbonate-based polyurethane elastomers: composition – property relationship, Eur. Polym. J. 47 (2011) 959–972, https://doi.org/10.1016/j.eurpolymj.2011.01.001.
[18] G. Kickelbick, Concepts for the incorporation of inorganic building blocks into organic polymers on a nanoscale, Prog. Polym. Sci. 28 (2003) 83–114, https://doi.org/10.1016/S0079-6700(02)00019-9.
[19] P.D. Lickiss, F. Rataboul, Fully condensed polyhedral oligosilsesquioxanes (POSS): from synthesis to application, in: A. Hill, M.J. Fink (Eds.), Advances in

Organometallic Chemistry, Vol. 57 Academic Press, 2008, pp. 1–116, , https://doi.org/10.1016/S0065-3055(08)00001-4.
[20] A.K. Nanda, D.A. Wicks, S.A. Madbouly, J.U. Otaigbe, Nanostructured polyurethane/POSS hybrid aqueous dispersions prepared by homogeneous solution polymerization, Macromolecules 39 (2006) 7037–7043, https://doi.org/10.1021/ma060809h.
[21] H. Honarkar, M. Barmar, M. Barikani, P. Shokrollahi, Synthesis and characterization of polyhedral oligomeric silsesquioxane-based waterborne polyurethane nanocomposites, Korean J. Chem. Eng. 33 (2016) 319–329, https://doi.org/10.1007/s11814-015-0102-2.
[22] Q. Zhang, X. Huang, X. Wang, X. Jia, K. Xi, Rheological study of the gelation of cross-linking polyhedral oligomeric silsesquioxanes (POSS)/PU composites, Polymer (United Kingdom) 55 (2014) 1282–1291, https://doi.org/10.1016/j.polymer.2014.01.040.
[23] J.P. Lewicki, K. Pielichowski, M. Jancia, E. Hebda, R.L.F. Albo, R.S. Maxwell, Degradative and morphological characterization of POSS modified nanohybrid polyurethane elastomers, Polym. Degrad. Stab. 104 (2014) 50–56, https://doi.org/10.1016/j.polymdegradstab.2014.03.025.
[24] B. Janowski, K. Pielichowski, Thermo(oxidative) stability of novel polyurethane/POSS nanohybrid elastomers, Thermochim. Acta 478 (2008) 51–53, https://doi.org/10.1016/j.tca.2008.08.015.
[25] A.K. Surca, A. Rauter, M. Rodošek, L. Slemenik Perše, M. Koželj, B. Orel, Modified bis-(3-(3-(3-triethoxysilyl)propyl)thioureido)propyl terminated poly(dimethylsiloxane)/POSS protective coatings on AA 2024, Prog. Org. Coatings 103 (2017) 1–14, https://doi.org/10.1016/j.porgcoat.2016.11.023.
[26] S.W. Kuo, F.C. Chang, POSS related polymer nanocomposites, Prog. Polym. Sci. 36 (2011) 1649–1696, https://doi.org/10.1016/j.progpolymsci.2011.05.002.
[27] M. Oaten, N.R. Choudhury, Silsesquioxane-urethane hybrid for thin film applications, Macromolecules 38 (2005) 6392–6401, https://doi.org/10.1021/ma0476543.
[28] G. Mirchandani, G. Waghoo, R. Parmar, S. Haseebuddin, S.K. Ghosh, F.P. Group, Oligomeric silsesquioxane reinforced polyurethane with enhanced coating performance, Prog. Org. Coatings 65 (2009) 444–449, https://doi.org/10.1016/j.porgcoat.2009.03.009.
[29] K.Y. Mya, Y. Wang, L. Shen, J. Xu, Y. Wu, X. Lu, C. He, Star-like polyurethane hybrids with functional cubic silsesquioxanes: preparation, morphology, and thermomechanical properties, J. Polym. Sci. A, Polym. Chem. 47 (2009) 4602–4616, https://doi.org/10.1002/pola.23512.
[30] H. Ghermezcheshme, M. Mohseni, H. Yahyaei, Use of nanoindentaion and nanoscratch experiments to reveal the mechanical behavior of POSS containing polyurethane nanocomposite coatings: the role of functionality, Tribol. Int. 88 (2015) 66–75, https://doi.org/10.1016/j.triboint.2015.02.023.
[31] A.M. Díez-Pascual, M.A. Gómez-Fatou, F. Ania, A. Flores, Nanoindentation in polymer nanocomposites, Prog. Mater. Sci. 67 (2015) 1–94, https://doi.org/10.1016/j.pmatsci.2014.06.002.
[32] A. Rauter, L. Slemenik Perše, B. Orel, B. Bengu, O. Sunetci, A. Šurca Vuk, *Ex situ* IR and Raman spectroscopy as a tool for studying the anticorrosion processes in (3-glycidoxypropyl)trimethoxysilane-based sol-gel coatings, J. Electroanal. Chem. 703 (2013) 97–107, https://doi.org/10.1016/j.jelechem.2013.05.015.
[33] M. Rodošek, A. Rauter, L. Slemenik Perše, D. Merl Kek, A. Šurca Vuk, Vibrational and corrosion properties of poly(dimethylsiloxane)-based protective coatings for AA 2024 modified with nanosized polyhedral oligomeric silsesquioxane, Corros. Sci. 85 (2014) 193–203, https://doi.org/10.1016/j.corsci.2014.04.019.
[34] C.J. van Oss, R.J. Good, M.K. Chaudhury, Additive and nonadditive surface tension components and the interpretation of contact angles, Langmuir 4 (1988) 884–891, https://doi.org/10.1021/la00082a018.
[35] K. Geng, F. Yang, T. Druffel, E.A. Grulke, Nanoindentation behavior of ultrathin polymeric films, Polymer (Guildf) 46 (2005) 11768–11772, https://doi.org/10.1016/j.polymer.2005.08.096.
[36] X.Q. Liu, Y.S. Wang, J.H. Zhu, Epoxy resin/polyurethane functionally graded material prepared by microwave irradiation, J. Appl. Polym. Sci. 94 (2004) 994–999, https://doi.org/10.1002/app.20755.
[37] L. Shen, L. Wang, T. Liu, C. He, Nanoindentation and morphological studies of epoxy nanocomposites, Macromol. Mater. Eng. 291 (2006) 1358–1366, https://doi.org/10.1002/mame.200600184.
[38] F. Faraldi, B. Cortese, D. Caschera, G. Di Carlo, C. Riccucci, T. de Caro, G.M. Ingo, Smart conservation methodology for the preservation of copper-based objects against the hazardous corrosion, Thin Solid Films 622 (2017) 130–135, https://doi.org/10.1016/j.tsf.2016.12.024.
[39] B. Du, O.K.C. Tsui, Q. Zhang, T. He, Study of elastic modulus and yield strength of polymer thin films using atomic force microscopy, Langmuir 17 (2001) 3286–3291, https://doi.org/10.1021/la001434a.
[40] R. Consiglio, N. Randall, B. Bellaton, J. von Stebut, The nano-scratch tester (NST) as a new tool for assessing the strength of ultrathin hard coatings and the mar resistance of polymer films, Thin Solid Films 332 (1998) 151–156, https://doi.org/10.1016/S0040-6090(98)00987-0.
[41] I. Jerman, M. Koželj, B. Orel, The effect of polyhedral oligomeric silsesquioxane dispersant and low surface energy additives on spectrally selective paint coatings with self-cleaning properties, Sol. Energy Mater. Sol. Cells 94 (2010) 232–245, https://doi.org/10.1016/j.solmat.2009.09.008.
[42] M. Rodošek, M. Koželj, L. Slemenik Perše, R. Cerc Korošec, M. Gaberšček, A.K. Surca, Protective coatings for AA 2024 based on cyclotetrasiloxane and various alkoxysilanes, Corros. Sci. 126 (2017) 55–68, https://doi.org/10.1016/j.corsci.2017.06.011.
[43] Y.X. Zhang, M. Huang, F. Li, Z.Q. Wen, Controlled synthesis of hierarchical CuO nanostructures for electrochemical capacitor electrodes, Int. J. Electrochem. Sci. 8 (2013) 8645–8661.
[44] H. Niu, Q. Yang, K. Tang, A new route to copper nitrate hydroxide microcrystals, Mater. Sci. Eng. B. 135 (2006) 172–175, https://doi.org/10.1016/j.mseb.2006.08.045.
[45] G.W. Poling, Infrared reflection studies of metal surfaces, J. Colloid Interface Sci. 34 (1970) 365–374.
[46] M.R. Johan, M.S.M. Suan, N.L. Hawari, H.A. Ching, Annealing effects on the properties of copper oxide thin films prepared by chemical deposition, Int. J. Electrochem. Sci. 6 (2011) 6094–6104, https://doi.org/10.1088/0268-1242/20/5/012.
[47] N. Serin, T. Serin, S. Horzum, Y. Celik, Annealing effects on the properties of copper oxide thin films prepared by chemical deposition, Semicond. Sci. Technol. 20 (2005) 398–401, https://doi.org/10.1088/0268-1242/20/5/012.
[48] C.N. Young, C.R. Clayton, J.H. Wynne, J.P. Yesinowski, G.C. Daniels, Physicochemical investigation of chemical paint removers. II: role and mechanism of phenol in the removal of polyurethane coatings, Prog. Org. Coatings 88 (2015) 212–219, https://doi.org/10.1016/j.porgcoat.2015.06.014.
[49] L. Muresan, S. Varvara, E. Stupnišek-Lisac, H. Otmačić, K. Marušić, S. Horvat-Kurbegović, L. Robbiola, K. Rahmouni, H. Takenouti, Protection of bronze covered with patina by innoxious organic substances, Electrochim. Acta 52 (2007) 7770–7779, https://doi.org/10.1016/j.electacta.2007.02.024.
[50] M. Gaberšček, S. Pejovnik, Time evolution of the impedance response of a passive film: a simple application to the Li / $SOCl_2$ system, J. Electrochem. Soc. 146 (1999) 933–940, https://doi.org/10.1149/1.1391702.
[51] G. Di Carlo, C. Giuliani, C. Riccucci, M. Pascucci, E. Messina, G. Fierro, M. Lavorgna, G.M. Ingo, Artificial patina formation onto copper-based alloys: chloride and sulphate induced corrosion processes, Appl. Surf. Sci. 421 (2017) 120–127, https://doi.org/10.1016/j.apsusc.2017.01.080.
[52] M.P. Casaletto, T. De Caro, G.M. Ingo, C. Riccucci, Production of reference “ancient” Cu-based alloys and their accelerated degradation methods, Appl. Phys. A 83 (2006) 617–622, https://doi.org/10.1007/s00339-006-3545-9.
[53] G.M. Ingo, T. De Caro, C. Riccucci, E. Angelini, S. Grassini, S. Balbi, P. Bernardini, D. Salvi, L. Bousselmi, A. Cilingiroglu, M. Gener, V.K. Gouda, O. Al Jarrah, S. Khosroff, Z. Mahdjoub, Z. Al Saad, W. El-Saddik, P. Vassiliou, Large scale investigation of chemical composition, structure and corrosion mechanism of bronze archeological artefacts from Mediterranean basin, Appl. Phys. A 83 (2006) 513–520, https://doi.org/10.1007/s00339-006-3550-z.
[54] D.A. Scott, Bronze disease: a review of some chemical problems and the role of relative humidity, J. Am. Inst. Conserv. 29 (1990) 193–206.
[55] D.M. Bastidas, M. Criado, S. Fajardo, V.M. La Iglesia, E. Cano, J.M. Bastidas, Copper deterioration: causes, diagnosis and risk minimisation, Int. Mater. Rev. 55 (2010) 99–127.
[56] G.M. Ingo, C. Riccucci, M. Lavorgna, M.S. De Luna, M. Pascucci, G. Di Carlo, Surface investigation of naturally corroded gilded copper-based objects, Appli. Surf. Sci. 387 (2016) 244–251, https://doi.org/10.1016/j.apsusc.2016.06.082.